Improved $MnCeO_x$ Systems for the Catalytic Wet Oxidation (CWO) of Phenol in Wastewater Streams

Francesco Arena,*,†,‡ Jacopo Negro,† Adolfo Parmaliana,† Lorenzo Spadaro,‡ and Giuseppe Trunfio†

Dipartimento di Chimica Industriale e Ingegneria dei Materiali, Università degli Studi di Messina, Salita Sperone 31, I-98166 S. Agata (Messina), Italy, and Istituto CNR-ITAE "Nicola Giordano", Salita S. Lucia 5, I-98126 S. Lucia (Messina), Italy

The effects of chemical composition, calcination temperature, and the addition of potassium on the physicochemical properties and reactivity of $MnCeO_x$ systems in the catalytic wet oxidation (CWO) of phenol with oxygen ($T_R = 373$ K; $P_R = 1.0$ MPa; $w_{cat}/w_{phenol} = 5$) have been addressed. Characterization data of "fresh" and "spent" catalysts signal the occurrence of a typically heterogeneous reaction path, the surface reaction between the adsorbed intermediate(s), and activated oxygen species being the rate-determining step (rds). Basic relationships among structural properties, the redox pattern, and CWO activity provide evidence of the main catalyst design requirements. A new synthesis route based on the redox−precipitation reactions of various Mn and Ce precursors then yields $MnCeO_x$ catalysts with improved physicochemical features and superior CWO activity, in comparison to conventional coprecipitated systems.

Introduction

The imperative need to preserve global water resources from ever-increasing industrial pollution, actually faced both through a continuous decrease of limits to emissions in wastewaters and a growing application of industrial process water recycling, has increased over the years the scientific and technological interest in the catalytic wet oxidation (CWO) with air/oxygen of substrates toxic and/or refractory to conventional biological treatments.[1−3] Although noble-metal catalysts (e.g., Ru, Ir, Pt, etc.) feature considerable CWO performance toward many organic compounds,[1,3] their lifetime is affected by fouling/poisoning deactivation phenomena, which is too expensive for widespread industrial application.[1] Then, the objective of developing low-cost alternatives recently prompted great research concern in the CWO pattern of oxide systems, primarily those based on copper[1,3−5] and manganese.[1−3,6−14]

Although copper-based systems are claimed to be very effective CWO catalysts toward various model compounds,[3] we have recently documented that the action of copper-based systems in the CWO of phenol is dependent mostly on the leaching of the active phase driving an effective, yet homogeneous, reaction path.[4,5] Therefore, $MnCeO_x$ catalysts represent, to date, the most promising alternative to noble-metal systems, because they could associate high activity and selectivity to an excellent resistance to leaching.[1,2,6−14] Generally, the CWO performance is dependent on the dispersion and average oxidation number (AON) of the active phase,[6−12] whereas the stability has been fairly related to the oxidation of carbon-containing deposits and the reversibility of the surface redox cycle.[10] Improving the redox pattern through a proper tuning of the structure and dispersion of the active phase is then a benchmark for enhancing the performance of the $MnCeO_x$ system.[1,2,6−14] Affecting the dispersion of the active species across the support, the preparation method determines the oxidation state of manganese and the "oxide−support" interaction, which is evidenced by synergetic effects of a ceria carrier on the redox features of the MnO_x phase.[1,2,6−14] Favoring the stabilization of higher Mn oxidation states, alkali doping (e.g., potassium, cesium) represents a further chance for upgrading the CWO performance of the title system.[8−13] However, Abecassis-Wolfovich et al. recently related the CWO activity toward phenol of bare and promoted (e.g., potassium, cesium, platinum, ruthenium) $MnCeO_x$ catalysts to high surface reactive adsorption (SRA) and catalyst adsorption capacity (CAC), which involves deactivation by fouling.[11,12] They indicated a regenerative oxidation treatment at temperatures higher than the reaction temperature to restore the initial activity level, claiming also that a better performance would arise from the stabilization of a crystalline Mn_5O_8 phase.[11,12]

Therefore, addressing the reaction mechanism and the main factors determining the CWO pattern of the $MnCeO_x$ system, this paper shows that a new synthesis route, which is based on "redox−precipitation" reactions of various Mn and Ce precursors, leads to *highly dispersed* catalysts with improved physicochemcial properties, in comparison to "conventional" coprecipitated catalysts. Larger surface exposure and enhanced dispersion and redox behavior of the active phase then account for a superior activity of redox-precipitated catalysts in the CWO of phenol under mild reaction conditions (reaction temperature and pressure of $T_R = 373$ K and $P_R = 1.0$ MPa, respectively).

Experimental Section

(A) $MnCeO_x$ Catalyst. $MnCeO_x$ catalysts with $Mn_{at}/Ce_{at} = 0.75$ (A) and 1.0 (B) were prepared using the conventional coprecipitation method, by adding a 10 wt % Na_2CO_3 solution to $Mn(NO_3)_2-Ce(NO_3)_3$ or $MnCl_2-CeCl_3$ precursors, which were dissolved in distilled water (pH ≅4.0).[6,9−14] After filtration and washing, all the samples were dried at 373 K (for 16 h) and further calcined in air (for 6 h) at temperatures in the range of $T_{calc} = 673-1273$ K. An aliquot of the dried samples was doped with potassium (4 wt %) via the incipient wetness method, using a KNO_3 aqueous solution. Thereafter, doped samples were dried at 373 K and calcined in air at 673 K (for 6 h).

A $MnCeO_x$ catalyst (Mn_{at}:$Ce_{at} = 1.0$) was also prepared via the new "redox−precipitation" route, according to the following

* To whom correspondence should be addressed. Tel.: +39 090 6765606. Fax: +39 090 393134. E-mail address: Francesco.Arena@unime.it.

† Dipartimento di Chimica Industriale e Ingegneria dei Materiali, Università degli Studi di Messina.

‡ Istituto CNR-ITAE "*Nicola Giordano*".

10.1021/ie0701118 CCC: $37.00
Published on Web 05/19/2007

Table 1. List of the Studied Catalysts

catalyst	Mn/Ce (at./at.)	Mn loading[a]	K loading (wt %)	calcination temperature, T_{calc} (K)	surface area, SA (m^2/g)	ceria particle size, d_{CeO_2}[b] (nm)	pore volume, PV (cm^3/g)	average pore diameter, APD[c] (nm)
A4	3/4	15.7		673	69	5	0.19	107
A5	3/4	15.7		873	50	10	0.15	237
A8	3/4	15.7		1073	25	27	0.10	414
A10	3/4	15.7		1273	16	32	0.02	567
KA4	3/4	15.1	4	673	30	5	0.18	328
B4	1/1	20.9		673	99	3	0.24	94
KB4	1/1	20.1	4	673	61	6	0.27	160
C4	1/1	20.7		673	154		0.49	85

[a] From XRF elemental analysis. [b] From the Scherrer equation, applied to the ⟨111⟩ reflection of the cerianite. [c] Calculated as APD = (4 × PV)/SA.

Table 2. Catalytic Wet Oxidation (CWO) of Phenol (T_R = 373 K, P_R = 1.0 MPa), Pseudo-First-Order Kinetic Constants of Phenol (k_{Phen}) and Total Organic Carbon (TOC) Removal (k_{TOC}), and Weight Loss (ΔW) of the "Spent" Catalyst Samples

	k_{Phen}		k_{TOC}		
catalyst	($L\ g_{cat}^{-1}\ h^{-1}$)	($L\ m_{cat}^{-2}\ h^{-1}$)	($L\ g_{cat}^{-1}\ h^{-1}$)	($L\ m_{cat}^{-2}\ h^{-1}$)	ΔW (%)
A4	3.9×10^{-1}	5.7×10^{-3}	1.8×10^{-1}	2.6×10^{-3}	17
A6	3.5×10^{-1}	7.0×10^{-3}	1.4×10^{-1}	2.7×10^{-3}	15
A8	1.3×10^{-1}	5.4×10^{-3}	3.6×10^{-2}	1.4×10^{-3}	13
A10	4.5×10^{-2}	2.8×10^{-3}	1.2×10^{-2}	7.3×10^{-4}	7
KA4	6.5×10^{-1}	2.2×10^{-2}	3.0×10^{-1}	9.9×10^{-3}	17
B4	5.6×10^{-1}	5.6×10^{-3}	4.9×10^{-1}	4.9×10^{-3}	18
KB4	1.5×10^{0}	2.5×10^{-2}	1.2×10^{0}	2.0×10^{-2}	19
C4	2.6×10^{0}	1.7×10^{-2}	2.1×10^{0}	1.4×10^{-2}	16

procedure.[15,16] An amount of the $KMnO_4$ precursor was titrated at 333 K under vigorous stirring with a solution of $Ce(NO_3)_3$ and $Mn(NO_3)_2$ precursors, keeping the pH constant (8.0 ± 0.3) via the addition of a 0.2 M KOH solution, according to the following reaction scheme:

$$MnO_4^- + 3e^- + 2H_2O \rightarrow MnO_2 + 4OH^- \quad (1)$$

$$Mn^{2+} + 2H_2O \rightarrow MnO_2 + 2e^- + 4H^+ \quad (2)$$

$$Ce^{3+} + 2H_2O \rightarrow CeO_2 + e^- + 4H^+ \quad (3)$$

After titration, the solid was digested at 333 K for 30 min and then filtered, washed with hot distilled water, dried at 373 K (for 16 h) and further calcined in air at 673 K (for 6 h).

The list of the studied samples and the relative physicochemical properties are presented in Table 1.

(B) Surface Area. Surface area (SA_{BET}) values were obtained from the nitrogen adsorption/desorption isotherm at 77 K, using a fully automated model ASAP 2010 gas adsorption system (Micromeritics Instruments). The isotherms were elaborated, according to the Brunauer−Emmett−Teller (BET) model equation, for the determination of the monolayer volume and surface area values.

(C) X-ray Diffraction. X-ray diffraction (XRD) analysis of powdered samples in the range of $2\theta = 10°-80°$ was performed with a scan step of 0.05°/s, using a Philips X-Pert diffractometer that was operating with a Ni β-filtered Cu K_α radiation at 40 kV and 30 mA. The average size of the ceria particles was calculated using the Scherrer equation.

(D) Transmission Electron Microscopy. Transmission electron microscopy (TEM) images were acquired using a PHILIPS CM12 microscope (point-to-point resolution = 3 Å). Catalyst samples, ultrasonically dispersed in isopropanol, were deposited over a thin carbon film that was supported on a standard copper grid.

(E) Temperature-Programmed Reduction. Temperature-programmed reduction (TPR) measurements in the temperature range of 293−1073 K were conducted using a 6% H_2/Ar mixture that was flowing at 60 mL/min (STP) into a linear microreactor (d_{int} = 4 mm) that contains a catalyst sample of ca. 30 mg and heated at the rate of 12 K/min. Before measurements, all the samples were pretreated in situ at 673 K for 30 min in a pure oxygen flow (30 STP mL/min).

(F) Thermogravimetry. Thermogravimetric (TG-DSC) analysis of the "used" samples was performed in a static air atmosphere with a heating rate of 5 K/min, using a Netzsch simultaneous thermal analysis instrument (model STA 409C).

(G) Catalyst Testing. Catalyst testing in the CWO of phenol at 373 K was conducted in a semibatch mode using a 0.25 L stirred (∼1000 rpm) autoclave that was equipped with a magnetically driven turbine impeller and fed with pure oxygen at the rate of 0.2 STP L/min (P_{tot} = 1.0 MPa, P_{O_2} = 0.9 MPa). The initial phenol concentration was set at 1000 (± 100) ppm and the catalyst load was set at 5000 ppm (w_{cat}/w_{phen} = 5).[6−9] Under such conditions, intraparticle mass-transfer resistances were negligible, according to the Weisz−Prater criterion:

$$\frac{r_{app}\rho_p(d_p/2)^2}{D_{eff}C_{phen,S}} \cong (0.2-0.8) \times 10^{-4} \quad (\ll 0.15)$$

Liquid reaction samples were analyzed with respect to pH, phenol (using high-performance liquid chromatography (HPLC)), total organic carbon (using a TOC analyzer), and manganese concentration (via atomic absorption spectroscopy (AAS)), whereas the "mineralization" activity of representative catalysts was also probed by bubbling the outlet gaseous stream in a stirred $Ba(OH)_2$ aqueous solution and weighing the precipitated $BaCO_3$ after filtration, washing, and drying at 373 K (for 16 h).

Results and Discussion

(A) Structure−Activity Relationships. Highlighting the effects of the calcination temperature (A), chemical composition (e.g., Mn:Ce ratio) and the addition of potassium (B), the activity data of various catalysts in the CWO of phenol at 373 K and 1.0 MPa are compared in Figure 1, in terms of phenol and TOC conversion versus reaction time. It is immediately evident that the CWO performance of the $MnCeO_x$ system (Mn_{at}/Ce_{at} = 0.75) is controlled by the calcination treatment, being depressed for temperatures in excess of 873 K. Indeed, samples A4 and A6 feature a similar catalytic activity, leading to a ca. 90%

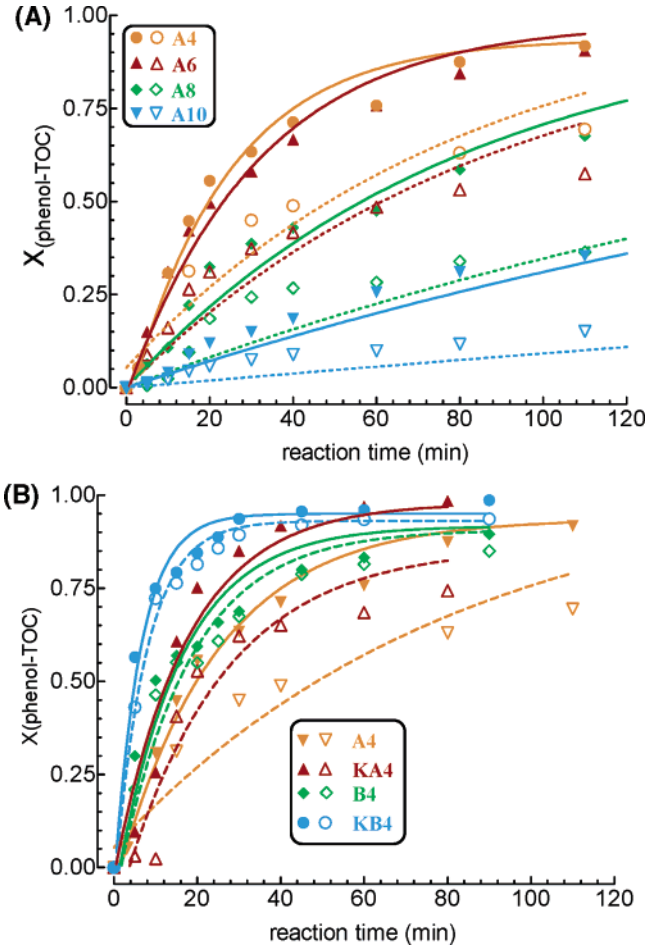

Figure 1. Activity data in the catalytic wet oxidation (CWO) of phenol (T_R = 373 K; P_R = 1.0 MPa; w_{cat}/w_{phen} = 5) of the coprecipitated catalysts (solid symbols represent phenol conversion, whereas open symbols represent TOC conversion; symbols denote samples as indicated in figure legend inset): (A) effect of the calcination temperature on the activity of the catalyst A and (B) effect of the Mn loading and K addition on the activity of the $MnCeO_x$ system calcined at 673 K.

phenol conversion in 2 h of reaction time and a final degree of TOC removal of 50%−60%. The sample calcined at 1073 K (sample A8) is less reactive, in the same time (2 h), which ensures phenol and TOC conversions of ca. 70% and ca. 30%, respectively, whereas, with conversion values of only 30% and 10%, the sample calcined at 1273 K (sample A10) features the poorest CWO performance.

Then, for a calcination temperature of T_{calc} = 673 K, an increase in the manganese loading (Mn_{at}/Ce_{at} = 1.0) visibly improves the CWO activity of the $MnCeO_x$ system,[1,2,6] because sample B4 features a comparable degree of conversion of the substrate (>90%) and, mostly, a much deeper (ca. 85%) TOC removal, in a shorter reaction time (90 min), with respect to sample A4 (see Figure 1B). However, the addition of potassium (4 wt %) promotes the CWO pattern of the A4 catalyst, accelerating the full phenol conversion in a time (80 min) even shorter than that of sample B4, although the TOC removal is slightly lower (ca. 75%). According to literature findings,[8,9,11,13] at least, the promoted KB4 system (Mn_{at}/Ce_{at} = 1.0) features the best CWO activity, resulting in the elimination of >90% of both phenol and TOC after just 30−40 min of reaction time (see Figure 1B).

Notably, despite a pH decrease to final values of ca. 4.5, caused by the ongoing degradation of the substrate into light

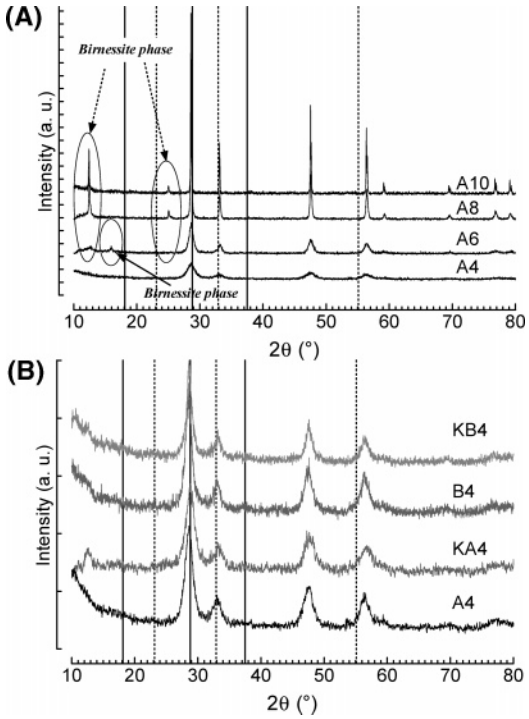

Figure 2. XRD patterns of the coprecipitated catalysts: (A) effect of the calcination temperature on the pattern of the catalyst A and (B) effect of the Mn/Ce ratio and K addition (4 wt %) on the pattern of the $MnCeO_x$ system calcined at 673 K.

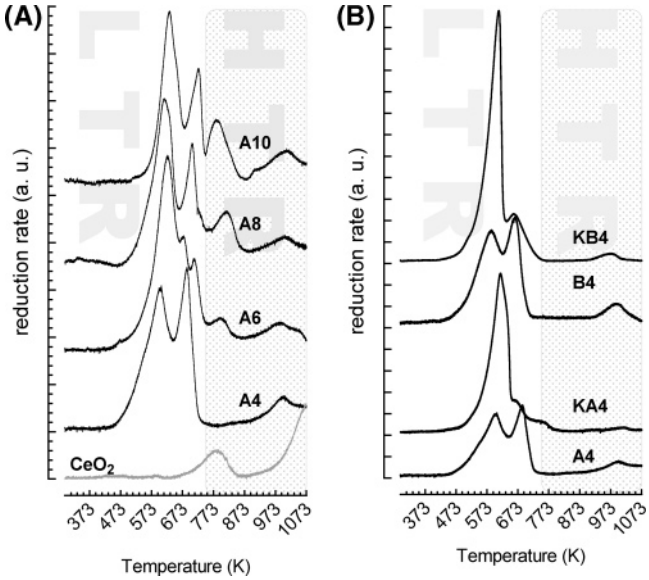

Figure 3. Temperature-programmed reduction (TPR) profiles of the coprecipitated catalysts normalized to the Mn loading: (A) effect of the calcination temperature on the pattern of the catalyst A and (B) effect of the Mn/Ce ratio and K addition (4 wt %) on the pattern of the $MnCeO_x$ system calcined at 673 K.

carboxylic acid intermediates (such as oxalic and formic acids),[1−6,13,14] all the catalysts are rather stable against leaching,[6−14] with the final concentration value of Mn ions in the reacting solution being on the order of a few ppm (2−5 ppm), corresponding to <1% of the total manganese load.

As evident from Figure 1, all the activity data obey, with satisfactory accuracy, the first-order reaction kinetics and, then, a quantitative comparison of the reactivity of the various catalysts can be made based on the kinetic constants of phenol (k_{phen}) and TOC (k_{TOC}) conversion:

$$\frac{dC_x}{dt} = k_x C_x[\text{Cat}]$$

The values of the kinetic constants, with reference to both catalyst weight (L g_{cat}^{-1} h^{-1}) and surface area (L m_{cat}^{-2} h^{-1}), along with the percentage weight loss recorded by TG-DSC analyses on the various "used" samples, are compared in Table 2. For the sake of comparison, such figures compare well with the k_{phen} values (0.46−1.2 L g_{cat}^{-1} h^{-1}) quoted by Abecassis-Wolfovich et al. for similar coprecipitated $MnCeO_x$ systems,[11,12] and then the intrinsic kinetic constants confirm the aforementioned reactivity scale:

$$\text{KB4} > \text{KA4} \approx \text{B4} \gg \text{A4} \approx \text{A6} > \text{A8} > \text{A10}$$

which is somewhat related to the surface area exposure (see Table 1). Indeed, the intrinsic activity of samples A4, A6, A8, and B4 is comparable, on a surface area unit basis, whereas the sample A8 and A10 systems exhibit a considerably lower reactivity, mostly for TOC removal. By contrast, as the surface area decreases (see Table 1), the intrinsic activity of K-promoted systems becomes superior to that of any undoped catalysts.[8,9,11,13] Furthermore, it can be noticed that the extent of weight loss of the "used" samples is somewhat related to the magnitude of the kinetic constants (see Table 2). In fact, catalyst samples A8 and A10, which are characterized by the smaller kinetic constants and partial conversion values (see Figure 1A), feature a weight loss of 13% and 7%, respectively, against an average value of 15%−17% of the other systems, ensuring complete conversion of the substrate (see Figure 1). Notably, these findings signal a quantitative adsorption of the substrate on the catalyst surface (phenol-to-catalyst mass ratio = 1/5), which evidently undergoes only a negligible conversion to CO_2.[10−13] As the mass-transport properties of the catalysts (Table 1) rule out the constraints of internal diffusion resistances on reaction kinetics, it can be stated that the relative abundance and chemical features of the surface phases/species control the SRA and CAC, previously taken as a measure of the CWO efficiency of the $MnCeO_x$ system.[10−12]

The XRD data of the various catalysts then are compared in Figure 2. The diffractograms of sample A calcined at different temperature (Figure 2A) always show the diffraction peaks (28.6°, 33.3°, 47.5°, 56.5°, 59.2°) of the cerianite with the fluorite-like structure. A sharper and more symmetric shape of such reflections confirms the growing degree of the crystallinity of samples calcined at higher T_{calc}, which is consistent with the surface area decay (see Table 1) induced by sintering.[17] Indeed, the fact that the average particle size of the ceria, calculated from the peak at 28.6° of the ⟨111⟩ crystal plane, is inversely related to the surface area (see Table 1), denotes the main contribution of the matrix to the surface area exposure.[12,17] Moreover, the appearance of small peaks at ca. 12.4° and 15.9° on sample A6 signals an incipient formation of a Na-birnessite phase (e.g., $Na_{0.7}MnO_2$),[18−20] which is evidently induced by the presence of a residual amount of Na ions coming from the coprecipitation stage. The concentration and crystallinity of such a species increases considerably until reaching a T_{calc} value of 1273 K, as indicated by the steep growth of reflections at 12.4° and 25.0° on samples A8 and A10 (see Figure 2A), which is likely related to the ⟨200⟩ and ⟨400⟩ crystal planes of a "O-richer" $Na_8Mn_{24}O_{48}$ phase.[18−20]

In addition to the reflections of the cerianite, the diffractogram of the B4 catalysts (see Figure 2B) shows a small peak at 37.5°, index of an incipient MnO_2 crystallization in the form of pyrolusite.[15,16,21] Whereas the addition of potassium, besides a small peak at 37.5°, causes the appearance of a small signal at 12.4°, index of an incipient formation of the K-birnessite structure.[18−20]

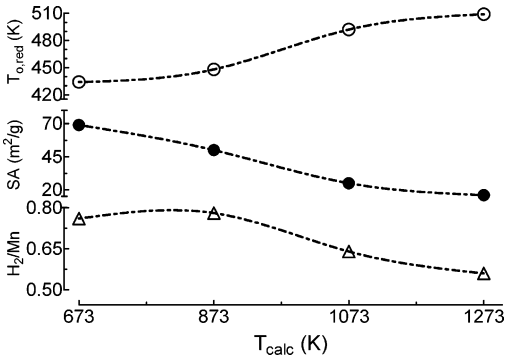

Figure 4. Effect of the calcination temperature (T_{calc}) on surface area (SA), onset of reduction temperature ($T_{o,red}$), and H_2/Mn ratio of catalyst A.

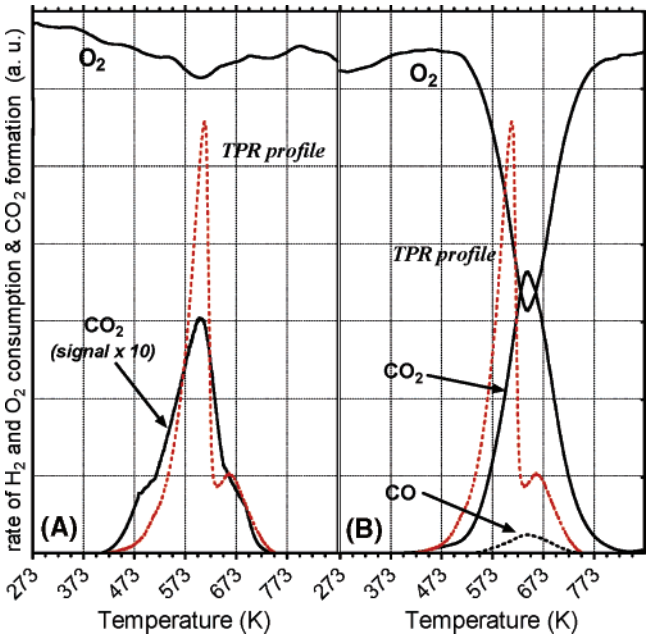

Figure 5. Comparison of the TPO profiles of (A) phenol (5 wt %) deposited on the "fresh" KB4 sample and (B) the "spent" KB4 catalyst, each relative to the TPR profile (Figure 3B) of the "as-prepared" system.

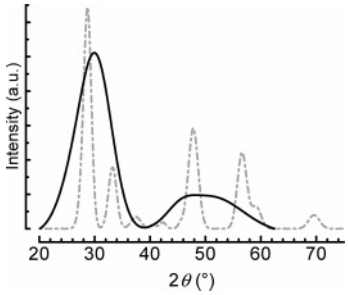

Figure 6. X-ray diffraction (XRD) pattern of catalyst C4.

We previously documented that a change in the structural properties, which is generally associated with a different surface exposure and dispersion of the active phase, reflects also on the redox behavior of MnO_x-based systems.[21] The results of TPR analysis then are shown in Figure 3, whereas the onset ($T_{o,red}$) and maximum (T_{Mi}) temperatures of reduction, along with the hydrogen consumption data, are summarized in Table 3. The calcination temperature provokes marked effects on the redox behavior of the A system, in qualitative and quantitative terms (Figure 3A), because a systematic shift of the onset

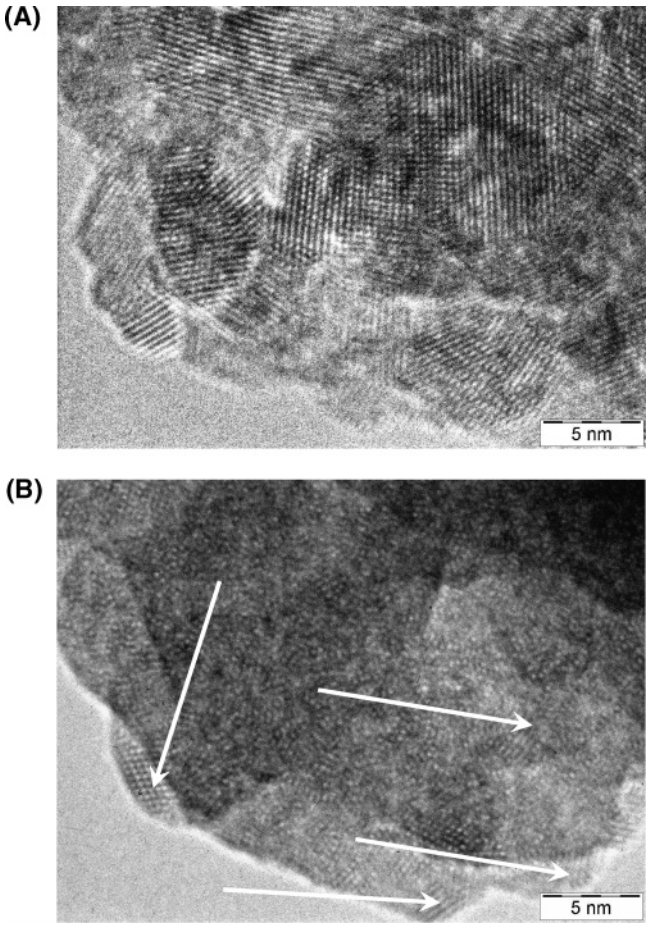

Figure 7. Transmission electron microscopy (TEM) images (920 000×) of the representative catalysts (A) B4 and (B) C4.

temperature of reduction with T_{calc} parallels an appreciable decrease in the extent of H_2 consumption in the lower temperature range (LTR) of 293−750 K. In fact, two or three peaks in such an LTR zone result from the reduction of Mn ions belonging to different structures/phases and/or with a different AON.[21] Sample A4 is the only sample that shows two reduction peaks, centered at 608 and 688 K, whose area corresponds to a H_2/Mn ratio of 0.76. They should be related to the reduction of very small MnO_2 particles that are well-dispersed across the ceria matrix (608 K) and to a fraction (ca. 50%) of Mn^{3+} cations belonging to a poor crystalline Mn_2O_3 phase, respectively.[21] Probably, the superposition of the main reflections with those of the ceria carrier and/or a low degree of crystallinity render such species undetectable on sample A4 via XRD analysis (see Figure 2A). The further hydrogen consumption in the higher temperature range (HTR), with a "smoothed" maximum (T_{M5}) at ca. 1000 K, is due to the ongoing bulk reduction of the ceria carrier.[4,15,16] Raising T_{calc} to 873 K (sample A6), the main reduction peak grows in intensity, keeping an almost unchanged position (T_{M1} = 625 K). According to XRD data, the other two small maxima on its descending side (LTR) can be attributed to the reduction of less reducible Mn_2O_3 (T_{M2} = 675 K) and Na-birnessite (T_{M3} = 710 K) species, respectively. While, in addition to the T_{M5} peak of the bulk reduction of ceria, another small resolved component at ca. 793 K (T_{M4}) in the HTR is associated with the reduction of surface Ce^{4+} ions.[4,15,16] The incipient formation of birnessite, the lack of reduction of surface Ce^{4+} ions in the LTR, and a larger fraction of the MnO_2 species account, overall, for the slight, if any, change in the H_2/Mn ratio (0.78). At higher T_{calc} (1073−1273 K), the T_{M1} peak (613−628 K) becomes sharper while a more intense T_{M3} component (708−728 K) matches the increasing concentration of birnessite (see Figure 2A). Overall, the H_2/Mn ratio decreases to 0.64 and 0.56 on the A8 and A10 catalyst samples, respectively. Therefore, such findings indicate a steady decrease of the catalyst reducibility at low temperature with increasing T_{calc}, due to lowering AON of Mn ions induced by MnO_x phase transformation and segregation. Perhaps a progressively more-evident peak at 787−813K, which is due to the reduction of surface Ce^{4+} ions (Figure 3A), supports the aforementioned statements.

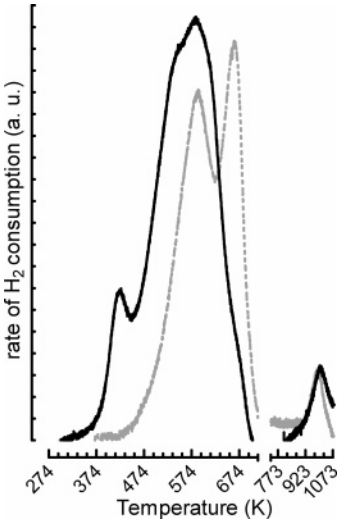

Figure 8. TPR profile of catalyst C4.

Therefore, higher surface area and dispersion of the active phase enhance the oxygen mobility and availability,[21] as documented by the similar decreasing trends of SA and H_2/Mn ratio with T_{calc}, and the specular rise of $T_{o,red}$, which is observed for the A system (Figure 4).

Inspecting the effects of the manganese loading and the addition of potassium on the reduction pattern of the $MnCeO_x$ system (Figure 3B), it can be observed that the temperature-programmed reduction (TPR) profile of sample B4 is substantially analogous to that of the A4 catalyst, because two main peaks centered at 590 and 663 K (LTR) account only for a larger H_2/Mn ratio (0.90). The addition of potassium to the A4 catalyst yields a strong increase of the intensity of the T_{M1} (606 K) peak and a decrease of the T_{M2}−T_{M3} components (see Table 3), leading to a value of H_2/Mn = 1.03.[8,9] Similarly, for the unpromoted systems, only slight differences can be found in the TPR pattern of sample KB4, in comparison to that of sample KA4, as the overwhelming intensity of the T_{M1} peak and a small T_{M2} band account for a H_2/Mn ratio of 1.06. In both cases, quantitative TPR data then would indicate a (partial) transformation of the Mn_2O_3 phase to a more or less crystalline MnO_2 and/or birnessite species (see Figure 2B), according to the tendency of alkaline dopants to stabilize higher oxidation states of the interacting oxide species.[8−13] Therefore, both textural and redox features, in turn, that are related to the dispersion of the active phase, are key issues of the CWO performance of $MnCeO_x$ systems. Namely, a large surface exposure drives the adsorption of the substrate at the catalyst surface while a high mobility availability of the oxygen catalyst should promote its subsequent conversion to CO_2. Slow gasification kinetics, testified by the weight loss close to the phenol-to-catalyst mass ratio, then remains the main drawback for the potential application of such catalysts to large-scale continuous processes.[1,2,12,13]

Table 3. Temperature-Programmed Reduction (TPR) Data of "Bare" and "K-Doped" Coprecipitated $MnCeO_x$ Catalysts

	Lower Temperature Range,LTR (293−750 K)					Higher Temperature Range,HTR (750−1073 K)		
catalyst	$T_{0,red}$ (K)	T_{M1} (K)	T_{M2} (K)	T_{M3} (K)	H_2/Mn_{at} (mol/atom)	T_{M4} (K)	T_{M5} (K)	H_2/Ce_{at} (mol/atom)
A4	434	608	688		0.76		1000	0.13
A6	448	625	675	710	0.72	793	985	0.15
A8	492	613		708	0.64	813	1000	0.22
A10	509	628		728	0.56	787	1010	0.26
B4	413	590	663		0.90		1000	0.15
KA4	410	617	662	750	1.03		990	0.17
KB4	410	610	662		1.06		1010	0.10

(B) Reaction Path. Considering that the adsorption of the substrate is the first preliminary step of the CWO reaction, we attempted to shed light onto the substrate−catalyst interaction pattern using gas-phase temperature-programmed oxidation (TPO) tests.[10] The TPO profiles of phenol (5 wt %) deposited by the incipient wetness on a "fresh" KB4 sample (Figure 5A), and that of the "used" KB4 sample (Figure 5B), are compared with the TPR pattern of the "as-prepared" catalyst in Figure 5. Analogous onset temperatures of reduction, O_2 consumption, and CO_2 formation signal that a close relationship exists between the rate of phenol oxidation and that of the catalyst reduction (see Figure 5A). In other words, these findings indicate that the catalyst oxygen mobility and availability, mediated by redox cycle(s) involving Mn ions, controls the rate of the surface oxidation step of the adsorbed substrate.[10] However, although the rate of phenol oxidation practically parallels that of catalyst reduction, attaining the maximum in concomitance with the maximum reduction rate (Figure 5A), the shift of the maximum of CO_2 formation to higher temperature on the "spent" sample (Figure 5B) is diagnostic of an incipient conversion of the substrate to less-reactive intermediates by side coupling/polymerization reactions.[1−3,6−14,22] Thus, the catalytic action of the $MnCeO_x$ system must involve the adsorption (step i) and the subsequent interaction of substrate/intermediates with the catalyst oxygen (steps ii−iv), prompting a reversible redox reaction cycle, "looped" by the gas-phase oxygen replenishing step (step v):[10]

$$\mathrm{Ph{-}OH} + \alpha \rightleftarrows \mathrm{Ph{-}OH}_{(s)} \quad \text{(i)}$$

$$\mathrm{Ph{-}OH}_{(s)} + \sigma\mathrm{{-}O} \rightarrow \mathrm{P}_{(s)} + \sigma \quad \text{(ii)}$$

$$\mathrm{P}_{(s)} \leftrightarrows \mathrm{P}_{(l)} \quad \text{(iii)}$$

$$\mathrm{P}_{(s)} + n(\sigma\mathrm{{-}O}) \rightarrow \mathrm{CO}_x \quad \text{(iv)}$$

$$\sigma + \mathrm{O}_2 \rightarrow \sigma\mathrm{{-}O} \quad \text{(v)}$$

(Here, "P" being a generic intermediate adsorbed ($P_{(s)}$) or released in the liquid phase ($P_{(l)}$), whereas "σ−O" and "σ" are the oxidized and reduced forms of active Mn sites, respectively). Furthermore, experimental findings indicate that the chemical composition and state of the active phase control the adsorption of the substrate, because faster kinetics of phenol and TOC removal of the promoted KA4 and KB4 catalysts (Table 2) could be linked to either a higher AON of the active phase and/or an improved surface affinity induced by potassium.[8−12] Therefore, it can be concluded that the CWO reaction of phenol proceeds via a typically heterogeneous "concerted" redox path promoted by an enhanced reducibility of the active phase,[10] because "Mn ←O" electron-transfer processes enable the formation of very reactive electrophilic oxygen species (e.g., O_2^-; $O_2^=$; O^-; $O^\bullet$) that are able to oxidize the substrate.[10] Structural, morphological, and redox properties of the active phase altogether determine the CWO activity and selectivity of the $MnCeO_x$ system, proving that key requirements of the catalyst design are improved textural and redox features to enhance the adsorption and the oxidative conversion of substrate/intermediate(s).[10]

(C) Catalyst Improvement. The objective of maximizing the surface area exposure and the dispersion of the active phase to enhance the redox activity and, consequently, the CWO performance,[6−13] pressed the design of an alternative synthesis route getting a mixture of the MnO_x and CeO_2 at an "atomic" level. Because the conventional coprecipitation technique leads to mixtures of "monophase" solid particles, because of the different solubility of the precipitating phases, a "cogeneration" of the MnO_2 and CeO_2 species further to "specific" reactions among proper precursors, was the main goal of the new preparation method.[15,16] Namely, "redox−precipitation" reactions of MnO_4^- with Ce^{3+}−Mn^{2+} ions in basic solution were exploited to attain a simultaneous formation of the MnO_2 and CeO_2 species, resulting in a very intimate dispersion of the two oxide components in the final catalyst.[15,16]

A preliminary evidence of the improved physicochemical properties of the $MnCeO_x$ catalyst obtained via the "redox−precipitation" route (C4 catalyst) is represented by a surface area exposure that is much larger than that of any coprecipitated systems (see Table 1).[15,16] This mirrors marked differences in the structural properties, as probed by the XRD pattern of the C4 catalyst (Figure 6), showing two unusually broad, "hill-shaped" reflections, spanning the ranges of 20°−38° and 40°−60°, respectively, with the former much more intense than the latter. Although the larger development of the total surface area, this peculiar diffractogram, typical of amorphous materials, cannot be only related to the different solid texture being, rather, the proof of an extremely homogeneous dispersion of MnO_x−CeO_2 species, hindering any "long-range" crystalline order.[15,16]

This is confirmed by TEM images of the representative B4 and C4 catalysts, shown in Figure 7. The former sample (Figure 7A) appears as an intricate array of "stepped" and randomly oriented crystalline domains (5−10 nm), characterized by the presence of ordered fringes with an estimated interatomic distance of 3.2 Å, which is typical of crystalline ceria.[15,16] On the other hand, the "redox-precipitated" system appears to be much more uniform, where a sporadic presence of crystalline ceria domains "encapsulated" into an amorphous matrix (Figure 7B), with an approximate size on the order of a few nanometers (3−5 nm), is hardly evident.[15,16] Thus, direct observations support the XRD evidence of a prevalently amorphous arrangement of the C4 system, which is due to a very intimate "sticking" of MnO_x and CeO_2 species.[15,16]

Such a very homogeneous dispersion of the active phase significantly affects the reduction pattern of the $MnCeO_x$ system, as shown in Figure 8. In comparison to the counterpart sample B4, sample C4 features a "narrower" profile, which is considerably shifted to lower temperature ($T_{o,red}$ = 293 K), bearing a main maximum at 583 K and a secondary one at ca. 543 K. Similar to that for samples A4 and B4, the former can be related to the reduction of very small MnO_2 particles, whereas that at lower temperature monitors the presence of "isolated" Mn^{4+}

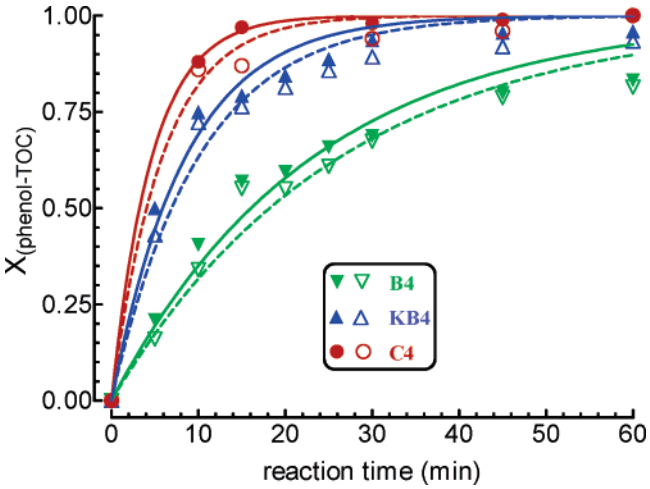

Figure 9. Activity data in the CWO of phenol (T_R = 373 K; P_R = 1.0 MPa; w_{cat}/w_{phen} = 5) of the "redox-precipitated" catalyst C4 (solid symbols represent phenol conversion, whereas open symbols represent TOC conversion; symbols denote samples as indicated in the figure legend inset).

ions, "embedded" into the surface defective positions of the ceria lattice. Their reduction is promoted by a high degree of coordinative unsaturation (CUS) and, perhaps, by neighboring Ce^{4+} ions, which, in turn, undergo reduction to Ce^{3+} species.[15,16] In addition, a resolved component centered at 422 K results from the reduction of very reactive oxygen species stabilized on the "isolated" Mn^{4+} ions.[15,16] This reduction pattern accounts for a greater extent of hydrogen consumption, resulting in a H_2/Mn ratio (1.06) comparable to that of the K-promoted systems (see Table 3). Then, even if a simultaneous partial reduction of surface Ce^{4+} ions could partially counterbalance the reduction of lower Mn-oxides, these findings are consistent with the higher dispersion and AON of the active phase greatly improving the oxygen capacity and mobility of the $MnCeO_x$ system in the range of 293−523 K.[15,16] Indeed, sample C4 misses the T_{M2} and T_{M3} components relative to reduction of Mn_2O_3 and birnessite species, whereas, in the spectrum of the coprecipitated system, the peaks at 420 and 543 K of "isolated" Mn^{4+} ions, at a much lower dispersion of the active phase, are almost absent.[15,16]

Comparing the CWO activity data of the coprecipitated B4 and KB4 catalysts with that of the "redox-precipitated" C4 system (Figure 9), it is evident that improved physicochemical properties yield a significant upgrade of the CWO performance. In particular, the C4 system features a much superior activity, in comparison to bare and K-promoted coprecipitated samples, resulting in a complete phenol and TOC removal in <15 min. In the same time, the KB4 catalyst attains a phenol conversion of ca. 75%, along with a <70% extent of TOC removal, whereas a complete disappearance of phenol occurs only after ca. 40 min in concomitance with a degree of TOC conversion of ca. 80%. Such data account for much-greater k_{phen} and k_{TOC} values, which are equal to 2.6 L g_{cat}^{-1} h^{-1} and 2.1 L g_{cat}^{-1} h^{-1}, respectively. These denote that the latter system is up to 5-fold more reactive than the coprecipitated B4 sample (k_{phen} = 0.56 L g_{cat}^{-1} h^{-1}; k_{TOC} = 0.49 L g_{cat}^{-1} h^{-1}) and almost twice as reactive (k_{phen} = 1.5 L g_{cat}^{-1} h^{-1}; k_{TOC} = 1.2 L g_{cat}^{-1} h^{-1}) as the promoted KB4 system (see Table 2). However, specific surface constants that are comparable to or lower than those of the promoted systems (see Table 2) signal that K^+ ions could enhance the surface affinity of the $MnCeO_x$ system toward the substrate.

At a minimum, TG-DSC characterization data of the "used" B4 and C4 catalysts are compared in Figure 10. Although a similar weight loss (15%−17%) indicates only a slight improvement in the mineralization activity under the adopted CWO conditions, the rate of CO_2 formation in the gas phase is considerably higher on the C4 catalyst, the maximum falling at a temperature (~523 K) appreciably lower than that of sample B4 (~563 K). This allows for a considerable narrowing of the temperature range for the complete oxidation of carbon-containing species on the former system. In agreement with the improved redox behavior (Figure 8), therefore, the major oxygen mobility of the C4 system in the temperature range of 293−523 K results in a comparatively superior oxidation strength than the counterpart sample B4, leading to a deeper oxidative degradation of the substrate under CWO conditions. This is confirmed by the (cumulative) amount of CO_2 formed during the CWO run, which resulted in an amount ~3 times higher for the "redox-precipitated" sample than for the coprecipitated one, accounting for CO_2 selectivity values of ca. 1.5% and 0.5%, respectively. Besides, despite the decrease in pH to 4.0−4.2, the extent of the Mn leaching at the end of the run was still negligible (<5 ppm), proving also a high chemical stability of the $MnCeO_x$ catalyst obtained via the new "redox−precipitation" route.[6−13]

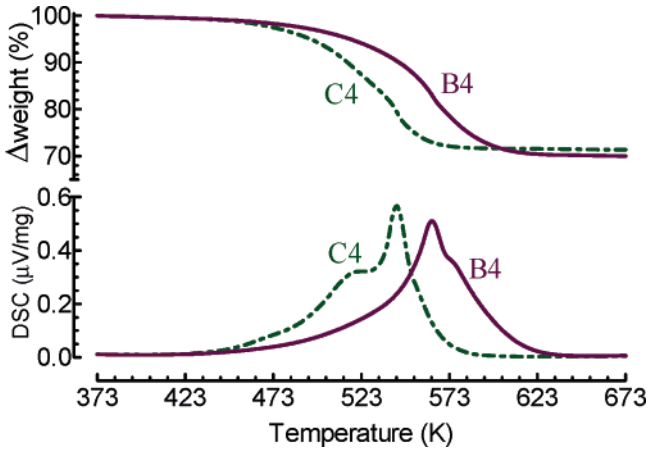

Figure 10. Thermogravimetry−differential scanning calorimetry (TG−DSC) analysis of the "spent" catalysts B4 and C4 (see Figure 9).

Conclusions

The effects of composition, calcination temperature, potassium addition, and preparation method on the physicochemical and catalytic pattern in the catalytic wet oxidation (CWO) of phenol of the $MnCeO_x$ system were addressed.

Textural, structural, and redox properties affect the CWO performance of the title system.

The CWO of phenol proceeds via a classic heterogeneous "redox" reaction path, with the surface reaction between adsorbed intermediates and activated oxygen species being the rate-determining step (rds).

The disclosed redox−precipitation route allows one to obtain highly dispersed $MnCeO_x$ systems with much-improved physicochemical properties, in comparison to conventional "coprecipitated" systems.

The redox−precipitation catalyst exhibits a superior performance in the CWO of phenol under "mild" reaction conditions, both in terms of activity and CO_2 selectivity.

Acknowledgment

The partial financial support by "A.R.P.A. SICILIA" (Palermo, Italy), in the framework of a research contract between "A.R.P.A. SICILIA" and "D.C.I.I.M.-U.M." (Messina, Italy) on

the topic, "Abatement of Organic Pollutants in Industrial and Civic Wastewaters by Catalytic Wet Air Oxidation (CWAO): Development of Active, Selective and Stable Catalysts" (July 2004/July 2006), is acknowledged. The authors also gratefully acknowledge Dr. F. Frusteri (Istituto CNR-ITAE "*Nicola Giordano*", Messina) for providing the TEM photographs.

Literature Cited

(1) Bhargava, S. K.; Tardio, J.; Prasad, J.; Föger, K.; Akolekar, D. B.; Grocott, S. C. Wet oxidation and catalytic wet oxidation. *Ind. Eng. Chem. Res.* **2006**, *45*, 1221.

(2) Larachi, F. Catalytic wet oxidation: micro-meso-macro methodology from catalyst synthesis to reactor design. *Top. Catal*. **2005**, *33*, 109.

(3) Matatov-Meytal, Y. I.; Sheintuch, M. Catalytic abatement of water pollutants. *Ind. Eng. Chem. Res.* **1998**, *37*, 309.

(4) Arena, F.; Giovenco, R.; Torre, T.; Venuto, A.; Parmaliana, A. Activity and resistance to leaching of Cu-based catalysts in the wet oxidation of phenol. *Appl. Catal., B* **2003**, *45*, 51.

(5) Arena, F.; Alongi, E.; Famulari, P.; Parmaliana, A.; Trunfio, G. Basic evaluation of the catalytic pattern of the $CuCeO_x$ system in the wet oxidation of phenol with oxygen. *Catal. Lett.* **2006**, *107*, 39.

(6) Chen, H.; Sayari, A.; Adnot, A.; Larachi, F. Composition−activity effects of Mn−Ce−O composites on phenol catalytic wet oxidation. *Appl. Catal., B* **2001**, *32*, 195.

(7) Hamoudi, S.; Larachi, F.; Sayari, A. Wet oxidation of phenolic solutions over heterogeneous catalysts: Degradation profile and catalyst behaviour. *J. Catal.* **1998**, *177*, 247.

(8) Hussain, S. T.; Sayari, A.; Larachi, F. Enhancing the stability of Mn−Ce−O WETOX catalysts using potassium. *Appl. Catal., B* **2001**, *34*, 1.

(9) Hussain, S. T.; Sayari, A.; Larachi, F. Novel K-Doped Mn−Ce−O Wet Oxidation Catalysts with Enhanced Stability. *J. Catal.* **2001**, *201*, 153.

(10) Arena, F.; Parmaliana, A.; Trunfio, G. Effects of chemical composition, preparation method and promoters on activity and stability of $MnCeO_x$-based catalysts for the CWO of phenol. In *Proceedings of the TOCAT 5 Conference*, Tokyo, July 23−28, 2006 (in press).

(11) Abecassis-Wolfovich, M.; Landau, M. V.; Brenner, A.; Herskowitz, M. Catalytic wet oxidation of phenol with Mn−Ce-based oxide catalysts: impact of reactive adsorption on TOC removal. *Ind. Eng. Chem. Res.* **2004**, *43*, 5089.

(12) Abecassis-Wolfovich, M.; Landau, M. V.; Brenner, A.; Herskowitz, M. Low-temperature combustion of 2,4,6-trichlorophenol in catalytic wet oxidation with nanocasted Mn-Ce-oxide catalyst. *J. Catal.* **2007**, *247*, 201.

(13) Santiago, A. F. J.; Sousa, J. F.; Guedes, R. C.; Jerônimo, C. E. M.; Benachour, M. Kinetic and wet oxidation of phenol catalyzed by non-promoted and potassium-promoted managnese/cerium oxide. *J. Hazard. Mater. B* **2006**, *38*, 325.

(14) Imamura, S. In *Catalysis by Ceria and Related Materials*; Trovarelli, A., Ed.; Imperial College Press: London, U.K., 2002; Vol. 14, p 431.

(15) Arena, F.; Trunfio, G.; Negro, J.; Spadaro, L. Synthesis of highly dispersed $MnCeO_x$ catalysts via a novel redox−precipitation route. *Mater. Res. Bull*. **2007**, in press.

(16) Arena, F.; Trunfio, G.; Negro, J.; Fazio, B.; Spadaro, L. Basic Evidence of the Molecular Dispersion of $MnCeO_x$ Catalysts Synthesized via a Novel "Redox-Precipitation" Route. *Chem. Mater.* **2007**, *19* (9), 2269−2276.

(17) Lin, X.-M.; Li, L.-P.; Li, G.-S.; Su, W.-H. Transport property and Raman spectra of nanocrystalline solid solutions $Ce_{0.8}Nd_{0.2}O_{2-\delta}$ with different particle size. *Mater. Chem. Phys.* **2001**, *69*, 236.

(18) Tsuda, M.; Arai, H.; Sakurai, Y. Improved cyclability of Na-birnessite partially substituted by cobalt. *J. Power Sources* **2002**, *110*, 52.

(19) Yang, L.-X.; Zhu, Y.-J.; Cheng, G.-F. Synthesis of well-crystallized birnessite using ethylene glycol as a reducing agent. *Mater. Res. Bull.* **2007**, *42*, 159.

(20) Xia, G.-G.; Tong, W.; Tolentino, E. N.; Duan, N.-G.; Brock, S. L.; Wang, J.-Y.; Suib, S. L. Synthesis and characterization of nanofibrous sodium manganese oxide with a 2×4 tunnel structure. *Chem. Mater*. **2001**, *13*, 1585.

(21) Arena, F.; Torre, T.; Raimondo, C.; Parmaliana, A. Structure and redox properties of bulk and supported manganese oxide catalysts. *Phys. Chem. Chem. Phys.* **2001**, *3*, 1911.

(22) Kim, S.-K.; Ihm, S.-K. Nature of carbonaceous deposits on the alumina supported transition metal oxide catalysts in the wet air oxidation of phenol. *Top. Catal.* **2005**, *33*, 171.

Received for review January 17, 2007
Revised manuscript received April 13, 2007
Accepted April 13, 2007

IE0701118